A Geometric Algorithm for Robust Multibody Inertial Parameter Identification

Taeyoon Lee and Frank C. Park

***Abstract*—Notwithstanding the seemingly straightforward nature of the inertial parameter identification problem for multibody systems—the most common formulation is as a linear least-squares estimation problem—existing methods, especially for complex high-dof systems subject to nonpersistent and noisy measurements, tend to be highly sensitive to the choice of initial values, and more often than not converge to ad hoc solutions that lie on arbitrary user-specified boundaries. We argue in this letter that such ill-posed behavior is traceable in large part to the use of the standard Euclidean metric in the regularized least-squares error criterion. We instead make use of the fact that the collection of inertial parameters constitutes a Riemannian manifold with a naturally defined Riemannian metric. By formulating and minimizing a coordinate-invariant error criterion based on this natural Riemannian metric, we show that accuracy and robustness of the identification can be vastly improved. Experiments involving high-dof humanoid structures are presented to validate our method and claims.**

***Index Terms*—Calibration and identification, dynamics.**

I. Introduction

THE identification of the mass and inertial parameters of a robot, and more generally of any system that can be modeled and represented as a rigid multibody system, e.g., digital characters and humans, is a prerequisite to any dynamic model-based method for motion planning and control. Not surprisingly, there is an extensive literature on methods for inertial parameter identification [1]–[5], also referred to as dynamic calibration in analogy to the even more well-studied problem of kinematic calibration. Nearly all of the previous approaches exploit the fact that a robot's dynamics are linear in the mass and inertial parameters; that is, for a n-link open chain with joint variables $q \in \mathbb{R}^n$ and joint torque vector $\tau \in \mathbb{R}^n$, the dynamic equations are of the form

$$\tau = M(q,\Phi)\ddot{q} + b(q,\dot{q},\Phi) = \Gamma(q,\dot{q},\ddot{q})\Phi, \tag{1}$$

where $\Phi \in \mathbb{R}^{10n}$ denotes the complete set of mass and inertial parameters for the n links, $M(q,\Phi) \in \mathbb{R}^{n\times n}$ is the mass matrix, and $b(q,\dot{q},\Phi) \in \mathbb{R}^n$ denotes the vector of Coriolis and gravitational forces; these terms can be collected and represented as $\Gamma(q,\dot{q},\ddot{q})\Phi$, where $\Gamma(q,\dot{q},\ddot{q}) \in \mathbb{R}^{n\times 10n}$.

Typical approaches to inertial parameter identification take measurements of τ, q, $\dot{q}$, $\ddot{q}$ at multiple points along some reference trajectory, and formulate the calibration problem as a least-squares estimation problem for Φ. One reason this problem is less than straightforward is that the link inertial parameters contained in Φ are subject to a rather unconventional set of positive-definiteness requirements (following [11], [10], we refer to these requirements as the *physical consistency* conditions). Further complicating matters is that for complex high-dof structures like humans and humanoids, the measurement data is often noisy and insufficient to reliably identify the entire set of parameters; the resulting ill-conditioning of the identification matrix is traceable in large part to the limited *persistency of excitation* of the reference trajectory.

The *physical consistency* requirements can be strictly guaranteed via a set of linear matrix inequality constraints, leading to a semidefinite programming problem [9], [10]; orthogonal decomposition-based manifold optimization techniques offer an alternate solution to this problem [11]. However, unless it happens that the unconstrained least squares minimizer is already physically consistent, solutions to these inequality constrained formulations will necessarily lie on the boundary of physical consistency, e.g., some of the resulting links may end up being flat along one or more dimensions, or reduce to a point mass or even zero mass. Such results can in fact be observed in some of the examples reported in [10] and [11].

For standard robots with six or fewer dofs, generating reference trajectories with sufficient *persistency of excitation* [7], [8] and finding physically consistent solutions is more often than not feasible. This is not the case for more complex, high-dof structures. For the humanoid structures treated in [7], [12], imposing user-specified bounds on, e.g., the link masses and the locations of mass centers, often leads to ad hoc solutions lying at one of the arbitrary user-specified bounds.

We claim that such ill-posed behavior is traceable in large part to the use of standard Euclidean distance metric (more

Manuscript received September 11, 2017; accepted January 5, 2018. Date of publication January 30, 2018; date of current version March 29, 2018. This letter was recommended for publication by Associate Editor P. Martinet and Editor D. Song upon evaluation of the reviewers' comments. This work was supported in part by Naver Laboratories, in part by ADD-ICMTC, in part by SNU-IAMD, in part by BK21+, in part by MI Technology Innovation Program 10048320, in part by the National Research Foundation of Korea under Grant NRF-2016R1A5A1938472, in part by MOTIE Technology Innovation Program under Grant 2017-10069072, and in part by SNU BMRR Center under Grant DAPA-UD130070ID. *(Corresponding author: Frank C. Park.)*

The authors are with the Department of Mechanical and Aerospace Engineering, Seoul National University, Seoul 08826, South Korea (e-mail: alex07143@snu.ac.kr; fcp@snu.ac.kr).

This letter has supplementary downloadable material available at http://ieeexplore.ieee.org, provided by the author. The video file, ral_motions_visualization.mp4, shows motion trajectories used for human inertial parameter identification experiment described in the paper. Also, it visualizes identified parameters from least squares based method and our method with equivalent uniform ellipsoids shown from multiple views. The XML-based file, identified_parameters.xlsx, contains numeric values of identified parameters of each link from our method and least sqaures based method. Player Information: VLC media player, Excel version 2007 and later. Packing List: ral_motions_visualization.mp4, identified_parameters.xlsx. The size of the video is 23.1 MB. Contact alex07143@snu.ac.kr for further questions about this work.

Digital Object Identifier 10.1109/LRA.2018.2799426

specifically, as a regularizer to an ill-posed least squares error criterion that doesn't account for prior information in a physically consistent and natural way). The key idea of our approach rests on the fact that the collection of inertial parameters constitutes a Riemannian manifold with a naturally defined Riemannian metric. Applying a one-to-one mapping between a link's inertial parameters and the space of 4×4 symmetric positive-definite matrices first pointed out in [10], in this letter we formulate and minimize a coordinate-invariant error criterion based on this natural Riemannian metric. Consequently, more robust and physically consistent estimation of the inertial parameters is achieved even from insufficient excitation, without imposing any user-specified bounds on the feasible parameter values. Our method and claims are validated via experiments involving high-dof humanoid structures; the results demonstrate that accuracy and robustness of the identification can be considerably improved with our method.

II. Conventional Least-Squares Based Inertial Parameter Identification

The dynamic equations (1) of a general rigid multibody system with n number of links are linear with respect to the inertial parameters $\Phi_b = [\phi_{b_1}^T, \dots \phi_{b_n}^T]^T \in \mathbb{R}^{10n}$, where

$$\begin{aligned}\phi_{b_i} &= \phi_{b_i}(m_i, h_{b_i}, I_{b_i}) \\ &= [m_i, h_{b_i}^T, I_{b_i}^{xx}, I_{b_i}^{yy}, I_{b_i}^{zz}, I_{b_i}^{xy}, I_{b_i}^{yz}, I_{b_i}^{zx}]^T \in \mathbb{R}^{10}\end{aligned}$$

is the vectorized representation of the inertial parameters of the ith rigid link with mass m_i, mass center position $p_{b_i} \in \mathbb{R}^3$, $h_{b_i} = m_i p_{b_i}$, and rotational inertia matrix $I_{b_i} \in \mathbb{R}^{3\times3}$, all represented with respect to the body-fixed frame $\{b_i\}$.

To identify the inertial parameters of the links, assume m joint/contact forces and torques/moments are measured at k time instances along some reference trajectory; at each time instant k one then has m equations linear in the inertial parameters. Stacking these equations for each of the k time instances, the problem of identifying Φ_b reduces to solving the system of linear equations

$$A\Phi_b = b, \tag{2}$$

where the measured forces/torques, and joint positions, velocities, and accelerations after appropriate filtering, are all encoded in $A \in \mathbb{R}^{km\times10n}$ and $b \in \mathbb{R}^{km}$.

Identifying the inertial parameters is complicated by the fact that Φ_b must satisfy a set of physical consistency conditions that we now describe. As pointed out in [6] and applied to inertial parameter identification in [11], the requirement that a rigid body's mass m be positive and its inertia matrix I_b be positive-definite is in fact a necessary, but not sufficient, condition; a sufficiency condition can be obtained from the fact that the mass density function $\rho : \mathbb{R}^3 \to \mathbb{R}_0^+$ must be everywhere nonnegative. In [10] this physical consistency condition is expressed in the following alternative but equivalent form: denoting the $n \times n$ real-symmetric matrices by $\mathcal{S}(n)$, define the 4×4 symmetric matrix $P_b \in \mathcal{S}(4)$ as

$$P_b = \int \begin{bmatrix}\vec{r}_b \\ 1\end{bmatrix}\begin{bmatrix}\vec{r}_b \\ 1\end{bmatrix}^T \rho(\vec{r}_b)\, dV_b = \begin{bmatrix}\Sigma_b & h_b \\ h_b^T & m\end{bmatrix}, \tag{3}$$

where the second moment matrix $\Sigma_b \in \mathcal{S}(3)$ is defined by $\Sigma_b = \int \vec{r}_b \vec{r}_b^T \rho(\vec{r}_b) dV_b$. It is then shown in [10] that the condition that P_b be positive-definite, i.e., $P_b \succ 0$, is equivalent to the physical consistency conditions described in [11]. More explicitly, defining the one-to-one linear mapping $f : \mathbb{R}^{10} \to \mathcal{S}(4)$ as

$$\begin{aligned}f(\phi_b) = P_b &= \begin{bmatrix}\frac{1}{2}\mathrm{tr}(I_b)\cdot\mathbf{1} - I_b & h_b \\ h_b^T & m\end{bmatrix} \in \mathcal{S}(4) \\ f^{-1}(P_b) &= \phi_b(m, h_b, \mathrm{tr}(\Sigma_b)\cdot\mathbf{1} - \Sigma_b) \in \mathbb{R}^{10},\end{aligned}$$

where $\Sigma_b = \frac{1}{2}\mathrm{tr}(I_b)\mathbf{1} - I_b$, the physical consistency conditions on $\phi_b \in \mathbb{R}^{10}$ can be identified with the requirement that $P_b = f(\phi_b) \in \mathcal{P}(4)$ be positive-definite.

Based on the above, we define the manifold $\mathcal{M}$ of the set of physically consistent inertial parameters for a single rigid body as follows:

$$\begin{aligned}\mathcal{M} &\simeq \{\phi_b \in \mathbb{R}^{10} : f(\phi_b) \succ 0\} \subset \mathbb{R}^{10} \\ &\simeq \{P_b \in \mathcal{S}(4) : P_b \succ 0\} = \mathcal{P}(4).\end{aligned}$$

The elements can be identified in both $\mathbb{R}^{10}$ and $\mathcal{P}(4)$, also for different choices of body-fixed reference frame $\{b\}$. For a multibody system with n rigid links, the space of physically consistent inertial parameters is given by the product space $\mathcal{M}^n \simeq \mathcal{P}(4)^n$.

In practice, inertial parameter identification is formulated as a constrained least-squares estimation problem of the form

$$\min_{\Phi_b} \underbrace{(A\Phi_b - b)^T\Sigma^{-1}(A\Phi_b - b)}_{\text{measurement error}} + \gamma \underbrace{\|\Phi_b - {}^0\Phi_b\|^2}_{\text{regularizer}}. \tag{4}$$

The first term represents the squared measurement error; elements of the diagonal matrix $\Sigma = \mathrm{diag}(\sigma_1^2, \dots, \sigma_{km}^2) \in \mathbb{R}^{km\times km}$ weight each of the residuals according to the uncertainty or variance of the measurements. If we have perfect measurements of a full rank matrix A, and b is subject to zero-mean Gaussian noise of covariance Σ, then the least-squares minimizer without the regularization term is known to be the maximum-likelihood solution with the desirable statistical property of being asymptotically unbiased. Since in practice A is neither full rank nor perfectly measured, the regularization term with scale factor γ is added to make the problem well-posed, and to keep the estimated parameter values close to the initial values ${}^0\Phi_b$. Ignoring the physical consistency constraints, the optimal least-squares solution can be expressed in closed form as $\Phi_b^{LS} = (A^T\Sigma^{-1}A + \gamma I)^{-1}(A^T\Sigma^{-1}b + \gamma\cdot{}^0\Phi_b)$. There is further a rich literature on least squares-based identification strategies focusing on measurement uncertainties [22, Chapter 15] and excitation trajectories [7], [8].

However, as has been observed also in the recent literature [9], [12], pure unconstrained least squares solutions are generally not reliable in terms of physical consistency, and attempts have been made toward obtaining physically consistent optimal solutions, i.e., from projection-based or recursive trial and error based methods (these and related methods are surveyed in [9]), to more recent methods based on orthogonal decomposition-based manifold optimization techniques [11], or imposing a set of linear matrix inequality (LMI) constraints on the link inertial parameters ϕ_{b_i} as $f(\phi_{b_i}) \succeq 0$ [9], [10] in the optimization formulation. The latter approach of imposing LMI guarantees not only physically consistent and global minimum solution, but also leads to a semidefinite programming problem, for which reliable and efficient numerical methods are widely available. However, as depicted in Fig. 1, the constrained solution Φ_b^{LS+LMI} may end up lying on the boundary of the manifold $\mathcal{M}^n$ (i.e., a

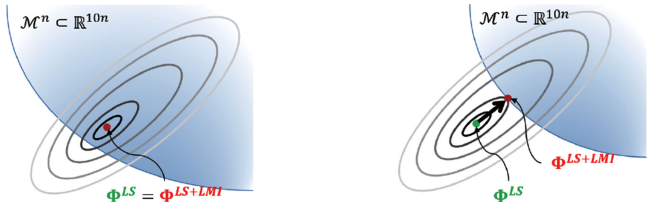

(a) $\Phi^{LS} \in \mathcal{M}^n$ (b) $\Phi^{LS} \in (\mathcal{M}^n)^c$

Fig. 1. The effect of imposing LMI while minimizing a least-squares objective function. The grey ellipsoidal contour indicates the least-squares objective function while the blue-shaded region is the feasible convex region of the search space in $\mathbb{R}^{10n}$ defined by the LMI. (a): When the pure least-squares minimizer Φ^{LS} is physically consistent, it coincides with the least squares minimizer subject to the LMI, Φ^{LS+LMI}. (b): When Φ^{LS} is not physically consistent, Φ^{LS+LMI} lies on the boundary of $\mathcal{M}^n$.

rank-deficient positive-semidefinite matrix P_{b_i}, leading to an ith rigid link that is, e.g., flat along one dimension, a point mass, or even zero mass) whenever the unconstrained global minimum Φ_b^{LS} lies outside $\mathcal{M}^n$ due to the convexity of the original objective function and the search space $\mathcal{M}^n \simeq P(4)^n$. The problem typically becomes even more pronounced for high-dof structures like humans and humanoids, and it is not uncommon to enforce stronger sufficiency conditions for physical consistency [7], [12], such as imposing user-specified convex bounds on, e.g., the link masses and the locations of mass centers.

However, most importantly, we claim that it is the use of the standard Euclidean distance metric, specifically as a regularizer to an ill-posed least squares error criterion that doesn't account for prior information in a physically consistent and natural way, that leads to a physically inconsistent unconstrained estimate Φ_b^{LS} despite small values of γ. Note in general that correctly incorporating the prior information becomes more critical for robust estimation when the measurement data is insufficient to identify the entire set of parameters. In line with the preceding discussion on the nature of the constrained solution, this implies that under the conventional regularized least squares formulation as in (4), imposing the physical consistency constraints generally will not improve matters much, and the solutions are highly susceptible to lying on the boundary of the user-specified feasible region. In the following section, we suggest an alternative objective function that is designed to fit $A\Phi_b = b$ in a more geometrically natural manner on $\mathcal{M}^n$, also without having to specify the physical consistency condition $f(\phi_{b_i}) \succeq 0$ as an explicit constraint.

III. An Intrinsic Riemannian Error Criterion

In this section, we frame the inertial parameter identification problem as an optimization problem on the Riemannian manifold $\mathcal{M}^n$. By exploiting the natural affine-invariant Riemannian structure of $\mathcal{M}^n$, a physically meaningful objective function can be formulated that is invariant with respect to choice of coordinate frames, and also to physical units and scales in a sense to be made precise below. We first review the Riemannian structure of $\mathcal{M}^n$ as a product space of $\mathcal{P}(4)$ endowed with an affine-invariant Riemannian metric. A distance metric $d_{\mathcal{M}^n}(\cdot,\cdot)$ on $\mathcal{M}^n$ is then constructed via the natural geodesic distance metric on $\mathcal{P}(4)$, and the corresponding objective function for inertial parameter identification is proposed. Details of the optimization algorithm are presented in the next section.

A. Riemannian Geometry of $\mathcal{P}(n)$

$\mathcal{P}(n)$, the space of real-symmetric $n \times n$ positive-definite matrices, is a manifold embedded in $\mathcal{S}(n)$ as an open and convex subset. Given a point $P \in \mathcal{P}(n)$, the tangent space at P, denoted $T_P\mathcal{P}(n)$, is $\mathcal{S}(n)$. For $P \in \mathcal{P}(n)$ and $V \in \mathcal{S}(n)$, the matrix logarithm map $\log : \mathcal{P}(n) \to \mathcal{S}(n)$ and matrix exponential map $\exp : \mathcal{S}(n) \to \mathcal{P}(n)$ defined by

$$\log(P) = -\sum_{k=1}^{\infty} \frac{(I-P)^k}{k} \quad \text{and} \quad \exp(V) = \sum_{k=0}^{\infty} \frac{V^k}{k!}$$

are both known to be unique and inverses of each other. For $P \in \mathcal{P}(n)$ and $X, Y \in T_P\mathcal{P}(n)$, the Riemannian metric invariant under the group action $G * P = GPG^T$, where $G \in GL(n)$ is any $n \times n$ nonsingular matrix, also called the affine-invariant metric [14], is given by

$$\langle X, Y \rangle_P = \frac{1}{2}\mathrm{tr}(P^{-1}XP^{-1}Y). \tag{5}$$

The geodesic at an arbitrary point $P \in \mathcal{P}(n)$ in the direction $V \in \mathcal{S}(n)$ can be obtained as

$$\gamma(t) = P^{1/2}\exp(tP^{-1/2}VP^{-1/2})P^{1/2}. \tag{6}$$

The exponential map of V at P, defined as $\gamma(1)$, is given by

$$\mathrm{Exp}_P(V) = P^{1/2}\exp(P^{-1/2}VP^{-1/2})P^{1/2}. \tag{7}$$

The logarithm map at P mapping a point $W \in \mathcal{P}(n)$ to the unique tangent vector V at P such that $\gamma(0) = P$, $\dot{\gamma}(0) = V$ and $\gamma(1) = W$, is given by

$$\mathrm{Log}_P(W) = V = P^{1/2}\log(P^{-1/2}WP^{-1/2})P^{1/2}. \tag{8}$$

The geodesic distance between two arbitrary points $P_1, P_2 \in \mathcal{P}(n)$, which can be calculated as the norm of $\mathrm{Log}_{P_1}(P_2)$ at P_1, is given by

$$d_{\mathcal{P}(n)}(P_1,P_2) = \|\mathrm{Log}_{P_1}(P_2)\|_{P_1} = \left(\sum_{i=1}^{n}\left(\log(\lambda_i)\right)^2\right)^{1/2}$$

where λ_i are the eigenvalues of $P_1^{-1/2}P_2P_1^{-1/2}$, or equivalently, those of $P_1^{-1}P_2$. It is straightforward to check that the geodesic distance $d_{\mathcal{P}(n)}(\cdot,\cdot)$ derived above from the affine-invariant Riemannian metric (5) is also invariant under the $GL(n)$ group action on P_1 and P_2.

B. Natural Distance Metric on $\mathcal{M}^n \simeq \mathcal{P}(4)^n$

Taking advantage of the fact that the manifold $\mathcal{M}$ of physically consistent inertial parameters of each link is equivalent to $\mathcal{P}(4)$, the manifold structure of of $\mathcal{M}^n$ is naturally inherited from that of $\mathcal{P}(4)$ defined in the former section. For two arbitrary physically consistent inertial parameters of a single rigid body ${}^1\phi_b, {}^2\phi_b \in \mathcal{M}$, we define the natural distance between them with $d_{\mathcal{P}(4)}$ as

$$d_{\mathcal{M}}({}^1\phi_b, {}^2\phi_b) = d_{\mathcal{P}(4)}({}^1P_b, {}^2P_b), \tag{9}$$

where ${}^iP_b = f({}^i\phi_b)$ for $i = 1, 2$. For an n-link multibody system, the distance metric can be defined via direct summation as $d_{\mathcal{M}^n}({}^1\Phi_b, {}^2\Phi_b) = \sum_{i=1}^{n} d_{\mathcal{M}}({}^1\phi_{b_i}, {}^2\phi_{b_i})$. We now show that this metric is coordinate frame-invariant.

Proposition 1: The metric $d_{\mathcal{M}}(\cdot,\cdot)$ defined in (9) is invariant with respect to choice of coordinate frames for representing the physical quantities in $\phi \in \mathcal{M}$.

Proof: Under a change of coordinate frame from $\{b\}$ to $\{a\}$, the relevant physical quantities transform according to the following rules:

$$\begin{aligned}\vec{r}_a &= \mathrm{diag}(d_{ab}^x, d_{ab}^y, d_{ab}^z)\cdot(R_{ab}\vec{r}_b + t_{ab}) \\ &= F_{ab}\vec{r}_b + g_{ab} \qquad (10)\\ \rho_a(\cdot)dV_a &= c_{ab}\cdot\rho_b(\cdot)dV_b, \qquad (11)\end{aligned}$$

where $d_{ab}^k \in \mathbb{R}^+$ and $c_{ab} \in \mathbb{R}^+$ are the change in physical scale/unit of length and mass, respectively, and $R_{ab} \in SO(3)$, $t_{ab} \in \mathbb{R}^3$ represent the rigid body transformation between frames a and b. Using the homogeneous representation of a 3-D vector, (10) can be rewritten as

$$\begin{bmatrix}\vec{r}_a \\ 1\end{bmatrix} = H_{ab}\cdot\begin{bmatrix}\vec{r}_b \\ 1\end{bmatrix}, \qquad (12)$$

where $H_{ab} \triangleq \begin{bmatrix}F_{ab} & g_{ab} \\ 0_{1\times 3} & 1\end{bmatrix} \in GL(4)$. Now from (3), (11), (12), the matrix representation of the inertial parameters P admits the following coordinate transformation rule in the form of a $GL(4)$ group action:

$$\begin{aligned}P_a &= \int \begin{bmatrix}\vec{r}_a \\ 1\end{bmatrix}\begin{bmatrix}\vec{r}_a \\ 1\end{bmatrix}^T \rho_a(\vec{r}_a)dV_a \\ &= c_{ab}\cdot H_{ab}\left(\int \begin{bmatrix}\vec{r}_b \\ 1\end{bmatrix}\begin{bmatrix}\vec{r}_b \\ 1\end{bmatrix}^T \rho_b(\vec{r}_b)dV_b\right)H_{ab}^T \\ &= c_{ab}\cdot H_{ab}P_bH_{ab}^T = G_{ab}P_bG_{ab}^T, \qquad (13)\end{aligned}$$

where $G_{ab} = \sqrt{c_{ab}}\cdot H_{ab} \in GL(4)$. Therefore, since the distance metric defined in (9) is invariant under the $GL(4)$ group action, it is also invariant to the choice of coordinate frame for representing the inertial parameter ϕ. ■

We now omit all the coordinate frame subscripts for expressing the inertial parameters ϕ and P.

Given inertial parameters $P(\Sigma, h, m) \in \mathcal{P}(4)$ of a single rigid body, we can construct a particular mass density function $\rho = m\bar{\rho}$ that realizes P by regarding $\bar{\rho}$ as a Gaussian density with mean $p = h/m$ and covariance $\bar{\Sigma}^C = \Sigma/m - pp^T$. Then P can be decomposed as

$$P = m\cdot\begin{bmatrix}\bar{\Sigma}^C + pp^T & p \\ p^T & 1\end{bmatrix} = m\cdot\bar{P}. \qquad (14)$$

The differential affine-invariant metric (5) on $\mathcal{P}(4)$ is given in terms of $(m, p, \bar{\Sigma}^C)$ by

$$\begin{aligned}ds^2 &= 2\left(\frac{dm}{m}\right)^2 + \frac{dm}{m}\cdot\mathrm{tr}\left((\bar{\Sigma}^C)^{-1}d\bar{\Sigma}^C\right) \\ &\quad + dp^T(\bar{\Sigma}^C)^{-1}dp + \frac{1}{2}\mathrm{tr}\left(\left((\bar{\Sigma}^C)^{-1}d\bar{\Sigma}^C\right)^2\right). \qquad (15)\end{aligned}$$

By inspection of each of the terms, it can be seen that the proposed metric offers a physical unit- and scale-free way of measuring distances on inertial parameters, which consist of diverse physical quantities (e.g., m [mass], h [mass·length], I [mass·length^2]). The robustness of our proposed identification algorithm is explained in large part by this property; typically there exist large discrepancies in sizes and masses between the links of a robot (e.g. base link vs end-effector for a robotic manipulator, hands/feet vs torso/thigh for a human or humanoid).

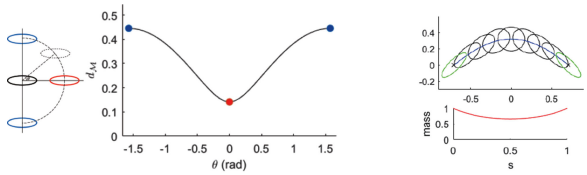

(a) Plot of geodesic distances between a pair of mass density functions (b) Geodesic path between two mass density functions

Fig. 2. Minimal geodesic distances and geodesic path on planar mass density functions under the natural metric. Each mass density function is visualized by an ellipse whose center and shape matches the center of mass and covariance matrix, respectively. (a) shows a plot of the distances from the fixed mass density function (black ellipse) to ones with the same mass and covariance, but constant deviation in positions of center of mass. (b) shows the geodesic path between two mass density functions (green ellipses).

To illustrate, the Euclidean distance between 15 kg and 13 kg is the same as the distance between 3 kg and 1 kg, which can make the estimation of link masses overly sensitive to lighter links. In (15), however, the small displacement in mass is normalized to a nondimensionalized value dm/m. Therefore, the distance between 3 kg and 1 kg would be measured to be much larger than the distance between 15 kg and 13 kg (about seven times larger), which in turn would naturally penalize more the deviation in mass of the lighter links in the estimation. Similar reasoning can also be applied for the size scale, since the distance between covariances is also defined in a scale-free way, thereby preventing relatively small rigid links to be estimated to a point mass. Using the Euclidean metric, one remedy could be to try to nondimensionalize each of the quantities by some representative constants. However, this requires the determination of the weights for each squared nondimensionalized quantity, for which there is no natural means of doing so.

We also note how the proposed metric measures distances and produces geodesic paths between mass density functions depending on the location of the center of mass p and covariance $\bar{\Sigma}^C$. Fig. 2 shows that deviations in the center of mass along directions of shorter radii of the covariance tend to produce larger distances between density functions. As shown in Fig. 2(a), the pair of density functions whose centers of masses are aligned along the major principal axes produces the shortest distance. Moreover, in Fig. 2(b), the initial and final directions of the minimal geodesics are both aligned toward the major principal axes. Such tendencies are actually a highly desirable property for treating inertial parameter data and an important distinction from using the Euclidean metric. For instance, if a given rigid body is known to have the shape of a long bar with unknown density distribution, then it is desirable for the estimated center of mass to deviate more along the stretched direction of the bar than the perpendicular direction. With the present distance metric, we can naturally take this into account in the estimation, while the Euclidean metric fails to do so.

Remark 1: We further note the close relation between the proposed metric and the Fisher information metric on multivariate normal distribution [15]. Note that the matrix $\bar{P}$ only contains information about the normal distribution $\bar{\rho}$ and resides in a submanifold of $\mathcal{P}(4)$ whose $(4,4)$ entry is fixed to 1. Let us define such a submanifold $\mathcal{N} \subset \mathcal{P}(4) \simeq \mathcal{M}$, which is actually equivalent to the statistical manifold of multivariate

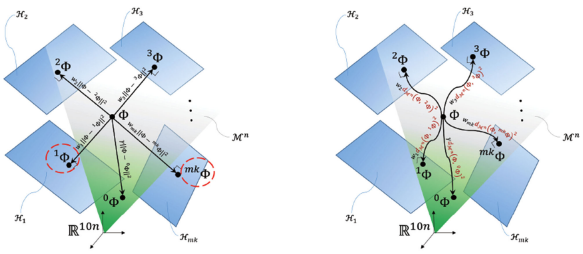

(a) Least-squares (b) Our formulation

Fig. 3. Pictorial description of the geometric meaning of the physically consistent inertial parameter identification problem. The green cone-shaped shaded region indicates the physically consistent manifold $\mathcal{M}^n$ embedded in $\mathbb{R}^{10n}$. The blue hyperplanes each represent the linear constraints in $A\Phi = b$. Each of the black arrows indicates the projection of Φ to the hyperplanes whose paths depend on the metric. Red dashed circles denote the projections of Φ to physically inconsistent values outside the green shaded region.

Gaussian distributions. Then the line element ds^2 induced onto the submanifold $\mathcal{N}$ can be expressed under $m = 1$ and $dm = 0$ as

$$ds^2_{\text{induced}} = dp^T(\bar{\Sigma}^C)^{-1}dp + \frac{1}{2}\text{tr}\left(\left((\bar{\Sigma}^C)^{-1}d\bar{\Sigma}^C\right)^2\right). \quad (16)$$

The induced metric (16) on $\mathcal{N}$ is exactly the Fisher information metric on the statistical manifold of multivariate normal distributions, widely used in information geometry as a coordinate-invariant Riemannian metric. Although $\mathcal{N}$ turns out to be non-geodesic submanifold of $\mathcal{M}$, it is of interest to note that the characteristics of the metric described in Fig. 2 correspond to the well-known ones of the Fisher information metric [16].

C. Intrinsic Distance-Based Least-Squares on $\mathcal{M}_n$

Identifying the physically consistent inertial parameters of a multibody system reduces to finding $\Phi \in \mathcal{M}^n \subset \mathbb{R}^{10n}$ that best fits the system of linear equations (2), $A\Phi = b$. Referring to Fig. 3, the problem can be equivalently restated in a geometrical way as finding Φ that is closest to each of the hyperplanes $\mathcal{H}_i \triangleq \{x \in \mathrm{R}^{10n} : a_i^T x = b_i\}, i = 1, \ldots, mk$, where $a_i \in \mathbb{R}^{10n}, b_i \in \mathbb{R}$ are the rows of A and b, respectively, and at the same time resides in $\mathcal{M}^n$. Viewed from this perspective, ordinary least-squares minimizes the weighted sum of squares of the Euclidean distances from Φ to each hyperplane and the prior value ${}^0\Phi$, i.e., referring to (4),

$$\min_{\Phi, \{{}^i\Phi\}_{i=1}^{mk}} \sum_{i=1}^{mk} w_i \|\Phi - {}^i\Phi\|^2 + \gamma\|\Phi - {}^0\Phi\|^2 \quad (17)$$

$$\text{s.t. } a_i^T {}^i\Phi = b_i, \quad i = 1, \ldots, mk, \quad (18)$$

where $w_i = \|a_i\|^2/\sigma_i^2$ and the ${}^i\Phi$ are a set of slack variables used in the equality-constrained optimization, physically corresponding to the projected points from Φ to each of the hyperplanes $\mathcal{H}_i$. Note however that the notion of projecting a point to the hyperplane depends on the metric defined on the space. As can be seen in (17) and (18), the least-squares formulation adopts an Euclidean metric on the parameter space; this can cause the projected points ${}^i\Phi$, marked as red dashed circles in Fig. 3(a), to be physically inconsistent. Since Φ eventually converges to the weighted arithmetic mean of ${}^i\Phi$s and ${}^0\Phi$, any physical inconsistencies in ${}^i\Phi$ can adversely affect the estimation of Φ.

The key idea in our approach is to use the natural metric on the physically consistent parameter space $\mathcal{M}^n$. The corresponding optimization problem formulation can be achieved by substituting the Euclidean norms $\|\cdot\|$ with the natural distance metric $d_{\mathcal{M}^n}(\cdot,\cdot)$:

$$\min_{\Phi, \{{}^i\Phi\}_{i=1}^{mk}} \sum_{i=1}^{mk} w_i \cdot d_{\mathcal{M}^n}(\Phi, {}^i\Phi)^2 + \gamma \cdot d_{\mathcal{M}^n}(\Phi, {}^0\Phi)^2 \quad (19)$$

$$\text{s.t. } \sum_{j=1}^{n} \text{tr}({}^iP_j\, {}^iX_j) = b_i, \quad i = 1, \ldots, mk, \quad (20)$$

where ${}^iP_j = f({}^i\phi_j) \in \mathcal{P}(4)$, and the constraint ${}^i\Phi \in \mathcal{H}_i$ is expressed in matrix form as (20) with ${}^iX_j \in \mathcal{S}(4)$, which is equivalent to vector constraints (18). With the proposed formulation, physical consistency can be guaranteed without explicitly constraining the parameters to be physically consistent, due to the well-defined metric-based projection and geometrical means on $\mathcal{M}^n$.

Remark 2: The squared measurement error in (4) is invariant to the linear transformations $\Phi \to M^{1/2}\Phi$ and $a_i \to M^{-1/2}a_i$ for any positive-definite matrix M. Therefore a constant dimensionless choice of $w_i = a_i^T M^{-1} a_i/\sigma_i^2$ with unique M satisfying $d\Phi^T M d\Phi \equiv \sum_{j=1}^{n}\langle f(d\phi_j), f(d\phi_j)\rangle_{f({}^0\phi_j)}$ is preferred over the choice $w_i = \|a_i\|^2/\sigma_i^2$.

Remark 3: Directly regularizing the linear least squares error with natural metric, e.g. $\min_\Phi \|A\Phi - b\|^2_{\Sigma^{-1}} + \gamma \cdot d_{\mathcal{M}^n}(\Phi, {}^0\Phi)^2$, is also possible, but the formulation (19), (20) provides a more geometrically intuitive algorithm as we argue below.

IV. Optimization Algorithm

The objective function (19) is minimized by an iterative cyclic optimization procedure, alternatively optimizing the slack variables $\{{}^i\Phi\}_{i=1}^{mk}$ and the inertial parameters Φ with an initial guess ${}^0\Phi$; geometrically this corresponds to repeated projection, and finding the means of the projected points. We now explain these two steps in more detail.

A. Optimizing $\{{}^i\Phi\}_{i=1}^{mk}$: Projection of Φ to $\mathcal{H}_i$

Given fixed Φ, each of the ${}^i\Phi$ can be optimized in parallel, each ${}^i\Phi$ updated via the following subproblem:

$${}^i\Phi = \arg\min_{\hat{\Phi}} \; d_{\mathcal{M}^n}(\Phi, \hat{\Phi})^2$$

$$\text{s.t. } \hat{\Phi} \in \mathcal{H}_i$$

which is exactly the definition of point-set projection in the metric space. However, it turns out that there exist multiple ($\sim O(2^{4n})$) of extremum points. Rather than exhaustively finding all possible extrema, the computational burden can be reduced by restricting the search space to the following neighborhood of Φ:

$$\mathcal{B}_\Phi = \{\hat{\Phi} \in \mathcal{M}^n : \lambda_{\max}(f(\phi_i)^{-1} f(\hat{\phi}_i)) \le e, \forall i = 1, \ldots, n\}.$$

It can be shown that there exists at most a single local minimum in $\mathcal{B}_\Phi$. In practice, most of the local minima ${}^i\Phi \in \mathcal{B}_\Phi$ are found to exist, except for cases where the measurement noise is excessive. We now propose the following point (Φ)-set ($\mathcal{H} \cap \mathcal{B}_\Phi$) projection rule on $\mathcal{M}^n$:

Proposition 2: The natural projection of $\Phi \in \mathcal{M}^n \subset \mathbb{R}^{10n}$ onto $\mathcal{H} \cap \mathcal{B}_\Phi$, where the hyperplane $\mathcal{H}$ is defined by $\mathcal{H} = \{x \in \mathbb{R}^{10n} : a^T x = b\} \simeq \{\{P_j\}_{j=1}^n \in \mathcal{S}(4)^n : \sum_{i=1}^n \mathrm{tr}(P_j X_j) = b\}$, is uniquely determined if and only if the monotonically decreasing function

$$\mathcal{C}(\lambda) = \sum_{j=1}^{n} \sum_{k=1}^{4} \sigma_j^k e^{-W(\lambda \sigma_j^k)} - b \tag{21}$$

has a unique root $\hat{\lambda}$ on the interval $[-g(\sigma_{\max}), g(-\sigma_{\min})]$, where $W(\cdot)$ is an inverse function of $w : [-1, \infty) \to \mathbb{R}$, $w(x) = xe^x$,

$$g(\sigma) = \begin{cases} 1/(e \cdot \sigma), & \text{if } \sigma > 0 \\ +\infty, & \text{otherwise} \end{cases}$$

σ_j^k are the eigenvalues of $\bar{X}_j = P_j^{1/2} X_j P_j^{1/2}$, and $\sigma_{\max}$, $\sigma_{\min}$ are the largest and smallest eigenvalues of $\{\bar{X}_j\}_{j=1}^n$.

Then the unique projected point $\hat{\Phi}$ is given by

$$\hat{\phi}_j = f^{-1}(\hat{P}_j) = f^{-1}(P_j^{1/2} e^{Q_j} P_j^{1/2}) \tag{22}$$

where $Q_j = R_j \cdot \mathrm{diag}(-W(\hat{\lambda}\sigma_j^k)) \cdot R_j^T$ and $R_j \in SO(4)$ is obtained from the eigendecomposition of $\bar{X}_j = R_j \Sigma R_j^T$.

Proof: The proof is given in the Appendix A. ■

Note that because of the monotonicity of $\mathcal{C}$, existence of the unique solution $\hat{\lambda}$ can be verified by simply evaluating $\mathcal{C}$ at the boundary of the specified interval. If the solution exists, the root is found numerically. Otherwise, the hyperplane $\mathcal{H}$ lies outside $\mathcal{M}^n$, or the projected point lies outside $\mathcal{B}_\Phi$, in which case the corresponding constraint is simply discarded at the initial stage.

B. Optimizing Φ: Geometric Mean of $\{{}^i\Phi\}_{i=1}^{mk}$

The optimal Φ given fixed $\{{}^i\Phi\}_{i=1}^n$ is obtained by solving an unconstrained optimization problem of the form

$$\Phi = \arg\min_{\hat{\Phi}} \sum_{i=1}^{mk} w_i \cdot d_{\mathcal{M}^n}(\hat{\Phi}, {}^i\Phi)^2 + \gamma \cdot d_{\mathcal{M}^n}(\hat{\Phi}, {}^0\Phi)^2, \tag{23}$$

which geometrically corresponds to the point that minimizes the weighted sum of squares of geodesic distances from $\{{}^i\Phi\}_{i=1}^n$ and ${}^0\Phi$. Therefore, the optimal Φ can be thought of as an extended version of the mean defined on the manifold; this same definition has been studied in the literature, known as a geometric mean [14] or Karcher mean [19]. The Karcher mean is known to uniquely exist for $\mathcal{P}(n)$. Moreover there exist gradient-based algorithms for numerically finding the Karcher mean. We use the Matlab function *manopt* [17] to solve (23).

V. Experiments on a Human Model

In this section we evaluate the performance of our inertial parameter identification algorithm on a high-dimensional human model. Unlike for actively controllable industrial robots, the number of measurable external or internal force/torques is limited, and the high number of inertial parameters of the system makes achieving persistent excitation challenging. Using a low-cost force plate (Wii balance board) that measures the vertical ground reactive force $f_z \in \mathbb{R}$ the ground position of the Zero Moment Point (ZMP) $(p_{zmp,x}, p_{zmp,y}) \in \mathbb{R}^2$, and a Kinect depth camera for kinematic tracking of the body links, we collect measurements on a human subject in motion, and compare the results of our algorithm with the LMI least-squares method of [10], i.e., $f(\phi_i) \succeq 0$, $i = 1, \ldots, n$. The results will allow us to assess how the identified solutions depend on the choice of error criterion subject to the same characterization of the feasible search space $\mathcal{M}^n \subset \mathbb{R}^{10n}$.

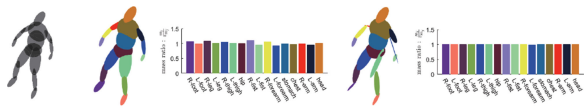

(a) Prior (b) Natural projection (c) Euclidean projection

Fig. 4. Projection results of inertial parameters to a single constraint from prior value. Equivalent ellipsoids for prior inertial parameters and projected ones are depicted in (a)–(c). Ratios of projected mass to prior values are also presented in (b) and (c).

Kinematic motion tracking is performed by fitting the SCAPE [13] articulated parametric human mesh model to the measured Kinect point cloud streams via the EM algorithm [18]. The tracked kinematic information is then post-processed by first filtering on $SE(3)$, and computing the spatial velocities and angular velocities of each of the links by finite difference method on $SE(3)$. The external force-moment measurements from the Wii balance board are synchronized with the Kinect measurements at a rate of 20–30 Hz. Prior inertial parameters ${}^0\Phi$ are calculated from the fitted SCAPE mesh model, assuming a constant mass density distribution over the whole body from the known total mass. The dynamic equations for identification that linearly relates the inertial parameters to the vertical ground reactive force, f_z, and moments, $m_y = -p_{zmp,x} \cdot f_z$ and $m_x = p_{zmp,y} \cdot f_z$, are derived in the Appendix B.

A. Projection of Inertial Parameters to a Single Constraint

To better focus on how the choice of metric affects the estimated inertial parameters, we compare how the inertial parameters are actually projected to a single constraint $\mathcal{H}$ from the prior ${}^0\Phi$ depending on the choice of metric. The human subject is asked to perform a short motion on the Wii balance board while facing the Kinect camera. Random sample is then taken of the measured data at a single time instance. We only consider the dynamic equation for m_x in (27) to obtain a single constraint. From the definition of point-set projection in metric space, the optimization problem can either be formulated as

$$\min_{\Phi} \ \|\Phi - {}^0\Phi\|^2 \quad \text{s.t. } \Phi \in \mathcal{H} \qquad \text{or} \qquad \min_{\Phi} \ d_{\mathcal{M}^n}(\Phi, {}^0\Phi) \quad \text{s.t. } \Phi \in \mathcal{H}$$

depending on the metric used. For the Euclidean projection, we impose an additional LMI constraint to ensure physical consistency of the projected parameter.

Fig. 4 shows the results of the projected inertial parameters depending on the choice of metric. Natural projection displays reasonable deviations from the prior value. In contrast, for the Euclidean metric the lengths of several principal axes of the equivalent ellipsoids collapse to zero, as predicted in our previous discussion on how lack of coordinate-invariance can cause scaling problems of this nature.

B. Identification of Inertial Parameters for Streaming Data

We now perform inertial parameter identification for streaming data. The human subject performs ten short motion

(a) Our method (b) LMI-based least-squares

Fig. 5. Identification results using our method and the LMI-based method are presented in (a) and (b), respectively. Equivalent ellipsoids of the identified inertial parameters together with mass deviations from prior values are shown.

TABLE I
COMPARISON OF RMSE ERROR OF PREDICTED MEASUREMENTS ($f_z\,[\mathrm{N}]$, $m_x\,[\mathrm{N}\cdot\mathrm{m}]$, $m_y\,[\mathrm{N}\cdot\mathrm{m}]$) AFTER IDENTIFICATION

	Identification			Validation		
	f_z	m_x	m_y	f_z	m_x	m_y
Prior	13.6	11.2	14.6	20.2	9.3	13.0
Our Method	15.7	4.8	11.7	21.3	6.8	10.5
Least Squares + LMI	13.7	5.5	12.6	20.3	7.7	11.5

sequences each for 3–4 seconds, with ground forces and ZMP positions sampled at approximately 100 time instances for the purposes of inertial parameter identification, and additional long motion sequences of 10 seconds performed for validation purposes. The resulting reference trajectory is still poorly excited with large condition number, i.e., $\mathrm{cond}(A^TA) = 9.53\cdot 10^6$. The regularization factor γ is set to be $\gamma = (10^{-2})\sum_{i=1}^{mk} w_i$, which is reasonably small considering that the proposed distance metric is of logarithmic scale. The LMI-based method took approximately 6.3 seconds to converge using CVX [20], while our method took approximately 23 minutes for convergence (both algorithms were implemented in matlab on an Intel Core i7-6700 computer).

As shown in Fig. 5(b), the identified parameters from the LMI-based method result in considerable errors, with many of the links estimated as point masses or flat in one or more dimensions. In spite of these obvious errors, the RMSE error of the predicted measurements, shown in Table I, turn out to be surprisingly similar to the ones obtained for our method and prior value, thereby implying that the identified parameters overfit the restricted motions observable from the available measurements. Prior information on the poorly excited parameters, which have small influence on the measurement error, is lost, which we again claim to be a consequence of Euclidean projection. In contrast, the identified parameters from our method are much more physically plausible. The size of the equivalent ellipsoids of the torso sharply increase, while the corresponding mass sharply decreases. This phenomenon can be explained from the observation that a large portion of the core part of the human torso is actually relatively low in density.

VI. CONCLUSION

Our main contribution lies in reformulating the classical linear least squares problem of inertial parameter identification to a nonlinear one, by exploiting the Riemannian geometry of the manifold of physically consistent inertial parameters. The robustness of our approach is traceable in large to the use of the natural Riemannian metric in lieu of the standard Euclidean metric. Our proposed metric can potentially be applied to developing more robust adaptation laws for robot adaptive control, in which the robot parameter values are estimated online from possibly non-persistent excitation trajectories.

As it stands, the main drawback of our algorithm is that it is considerably more computationally intensive than conventional Euclidean least-squares based methods (although since calibration is generally performed offline before operation of the robot, this issue may be less critical than, e.g., using our metric for adaptive control). Further work on developing parallel processing implementations of our algorithm, or relaxation methods, e.g., convex approximation, would mitigate these computational limitations to some extent.

Lastly, inclusion of friction, elasticity and other unmodeled effects into our identification framework is the target of future work for actual robots.

APPENDIX A
PROOF OF PROPOSITION 2

The Lagrangian for $\hat{\Phi} \sim \{\hat{P}_j\}_{j=1}^n$ can be defined as

$$\mathcal{L}(\{\hat{P}_j\}_{j=1}^n, \lambda) = \sum_{j=1}^{n} \frac{1}{2} d_{\mathcal{P}(4)}(P_j, \hat{P}_j)^2 + \lambda \left(b - \sum_{j=1}^{n} \mathrm{tr}(\hat{P}_j X_j) \right)$$

where λ is the Lagrange multiplier. Then for all admissible curves $c_j : \mathbb{R} \to \mathcal{P}(4)$, $j = 1, \ldots, n$ such that $c_j(0) = \hat{P}_j$ and $\dot{c}_j(0) = V_j \in \mathcal{S}(4)$, $\frac{d}{dt}|_{t=0}\mathcal{L}(\{c_j(t)\}_{j=1}^n, \lambda) = 0$ should hold as the first-order necessary condition. Since $\frac{d}{dt}|_{t=0} d_{\mathcal{P}(4)}(P_j, c_j(t))^2 = \langle \mathrm{Log}_{\hat{P}_j}(P_j), V_j \rangle_{\hat{P}_j}$ holds [19], we have $\sum_{j=1}^n \langle \mathrm{Log}_{\hat{P}_j}(P_j) - \lambda \cdot \hat{P}_j X_j \hat{P}_j, V_j \rangle_{\hat{P}_j} = 0$, which should hold for all variations of V_j. Therefore the first-order necessary condition is given by

$$\mathrm{Log}_{\hat{P}_j}(P_j) = \lambda \cdot \hat{P}_j X_j \hat{P}_j, \quad j = 1, \ldots, n.$$

Define $Q_j \triangleq \log(P_j^{-1/2} \hat{P}_j P_j^{-1/2}) \in \mathcal{S}(4)$, which also implies $\hat{P}_j = P_j^{1/2} e^{Q_j} P_j^{1/2}$. Then the first-order necessary condition further simplifies to

$$(-Q_j) e^{-Q_j} = \lambda \bar{X}_j, \quad j = 1, \ldots, n. \tag{24}$$

Let the eigendecomposition of $-Q_j \in \mathcal{S}(4)$ be $-Q_j = R_j \Gamma_j R_j^T$, where $\Gamma_j = \mathrm{diag}(\gamma_j^1, \ldots, \gamma_j^4)$. Then (24) becomes $\Gamma_j e^{\Gamma_j} = \mathrm{diag}(\gamma_j^1 e^{\gamma_j^1}, \ldots, \gamma_j^4 e^{\gamma_j^4}) = \lambda R_j^T \bar{X}_j R_j$, which implies that the matrix on the right-hand side is diagonal, and leads to the eigendecomposition of $\bar{X}_j$ to be of the form $\bar{X}_j = R_j \Sigma_j R_j^T$, where $\Sigma_j = \mathrm{diag}(\sigma_j^1, \ldots, \sigma_j^4)$. Then γ_j^k is the solution of

$$\gamma_j^k e^{\gamma_j^k} = \lambda \sigma_j^k,$$

which is given by $\gamma_j^k = W(\lambda \sigma_j^k)$ from the definition of W, also referred to as the Lambert W function. Note that there exists two solutions γ_j^k when $\lambda \sigma_j^k \in (-1/e, 0)$, one greater than -1, $W(\lambda \sigma_j^k)$, and the smaller $W_0(\lambda \sigma_j^k)$. However, since $\gamma_j^k = -\log(\lambda_k(P_j^{-1}\hat{P}_j)) \geq -\log(e) = -1$ from the restriction that $\hat{\Phi} \in \mathcal{B}_\Phi$, a monotonically increasing inverse function W defined on the interval $[-1/e, \infty)$ is the only one of interest. For the solution γ_j^k to exist, $\lambda \sigma_j^k \geq -1/e$ should hold for all $j = 1, \ldots, n$ and $k = 1, \ldots, 4$. This condition can equivalently be stated as $\lambda \in [-g(\sigma_{\max}), g(-\sigma_{\min})]$.

Meanwhile, $\sum_{j=1}^{n} \mathrm{tr}(X_j \hat{P}_j) = \sum_{j=1}^{n} \mathrm{tr}(\bar{X}_j e^{Q_j}) = \sum_{j=1}^{n} \mathrm{tr}(\Sigma_j e^{-\Gamma_j}) = \sum_{j=1}^{n} \sum_{k=1}^{4} \sigma_j^k e^{-W(\lambda \sigma_j^k)} = b$, which is exactly $\mathcal{C}(\lambda) = 0$. $\mathcal{C}(\cdot)$ is clearly a monotonically decreasing function from the monotonicity of $W(\cdot)$.

In summary, the necessary condition for the optimal solution $\hat{\Phi} \in \mathcal{B}_\Phi$ to exist can be transformed into the existence of a unique solution $\hat{\lambda} \in [-g(\sigma_{\max}), g(-\sigma_{\min})]$ to $\mathcal{C}(\lambda) = 0$. If such a solution exists, $\hat{\phi}_j$ is given by (22); the solution is in fact a local minima by the given convex invariant objective function [23] and linear constraint with respect to $P_j^{-1/2} \hat{P}_j P_j^{-1/2}$, whose eigenvalues are bounded on the interval $(0, \mathrm{e}]$ from the restriction $\hat{\Phi} \in \mathcal{B}_\Phi$.

APPENDIX B
FORMULATION OF DYNAMIC MODEL USED IN SECTION V

We utilize the fact that the net external force to the floating base multibody system is the time derivative of the total momentum. Setting the fixed reference frame $\{s\}$ with its z-axis normal to ground, the dynamic equations can be derived as in [21]:

$$F_s^{ext} + F_s^{grav} = \sum_{i=1}^{n} [\mathrm{Ad}_{T_{si}^{-1}}]^T (G_i \dot{V}_i - [\mathrm{ad}_{V_i}]^T G_i V_i), \quad (25)$$

where $F_s^{ext} = (m, f) \in dse(3)$ is the net external force from the ground, $F_s^{grav} = \sum_{i=1}^{n} [\mathrm{Ad}_{T_{si}^{-1}}]^T G_i [\mathrm{Ad}_{T_{si}^{-1}}] g_s$ is the gravitational force with constant gravitational acceleration vector $g_s = (0, a_s) \in se(3)$, $T_{si} \in SE(3)$ is the transformation from $\{s\}$ to the body frame of the ith link, $G_i(\phi_i) \in \mathbb{R}^{6\times6}$ is the constant inertia tensor for the ith link, and $V_i \in se(3)$ is the spatial body velocity of the ith link. Equation (25) can be written in linear form with respect to the inertial parameters as

$$F_s^{ext} = \Gamma\big(\{T_{si}, V_i, \dot{V}_i\}_{i=1}^{n}\big) \cdot \Phi, \quad (26)$$

with matrix $\Gamma \in \mathbb{R}^{6\times10n}$. In the present application, only the measurements of m_x, m_y, f_z are available. Therefore, the reduced set of linear equations for dynamic identification are derived as

$$\hat{F} = [m_x, m_y, f_z]^T = \hat{\Gamma}\big(\{T_{si}, V_i, \dot{V}_i\}_{i=1}^{n}\big) \cdot \Phi \in \mathbb{R}^3, \quad (27)$$

where $\hat{\Gamma} = S \cdot \Gamma \in \mathbb{R}^{3\times10n}$ and $S \in \mathbb{R}^{3\times6}$ is a constant selection matrix with entries 0 or 1, satisfying $\hat{F} = S F_s^{ext}$.

REFERENCES

[1] C. G. Atkeson, C. H. An, and J. M. Hollerbach., "Estimation of inertial parameters of manipulator lads and links," *Int. J. Robot. Res.*, vol. 5, no. 3, pp. 101–119, 1986.

[2] P. K. Khosla and T. Kanade, "Parameter identification of robot dynamics," in *Proc. 24th IEEE Conf. Decis. Control*, 1985, pp. 1754–1760.

[3] M. Gautier and W. Khalil, "On the identification of the inertial parameters of robots," in *Proc. 27th IEEE Conf. Decis. Control*, 1988, vol. 3, pp. 2264–2269.

[4] M. Mistry, S. Schaal, and K. Yamane, "Inertial parameter estimation of floating base humanoid systems using partial force sensing," in *Proc. 9th IEEE-RAS Int. Conf. Humanoid Robots*, 2009, pp. 492–497.

[5] K. Ayusawa, G. Venture, and Y. Nakamura, "Identifiability and identification of inertial parameters using the underactuated base-link dynamics for legged multibody systems," *Int. J. Robot. Res.*, vol. 33, no. 3, pp. 446–468, 2014.

[6] J. Wittenburg, *Dynamics of Multibody Systems*. Berlin, Germany: Springer-Verlag, 2007.

[7] V. Bonnet, P. Fraisse, A. Crosnier, M. Gautier, A. Gonzalez, and G. Venture, "Optimal exciting dance for identifying inertial parameters of an anthropomorphic Structure," *IEEE Trans. Robot.*, vol. 32, no. 4, pp. 823–836, Aug. 2016.

[8] A. D. Wilson, J. A. Schultz, and T. D. Murphey, "Trajectory synthesis for Fisher information maximization," *IEEE Trans. Robot.*, vol. 30, no. 6, pp. 1358–1370, Dec. 2014.

[9] C. D. Sousa and R. Cortesao, "Physical feasibility of robot base inertial parameter identification: A linear matrix inequality approach," *Int. J. Robot. Res.*, vol. 33, no. 6, pp. 931–944, 2014.

[10] P. M. Wensing, S. Kim, and J. J. E. Slotine, "Linear matrix inequalities for physically consistent inertial parameter identification: A statistical perspective on the mass distribution," *IEEE Robot. Autom. Lett.*, vol. 3, no. 1, pp. 60–67, Jan. 2018.

[11] S. Traversaro, S. Brossette, A. Escande, and F. Nori, "Identification of fully physical consistent inertial parameters using optimization on manifolds," in *Proc. 2016 IEEE/RSJ Int. Conf. Intell. Robots Syst.*, 2016, pp. 5446–5451.

[12] J. Jovic, A. Escande, K. Ayusawa, E. Yoshida, A. Kheddar, and G. Venture, "Humanoid and human inertia parameter identification using hierarchical optimization," *IEEE Trans. Robot.*, vol. 32, no. 3, pp. 726–735, Jun. 2016.

[13] D. Anguelov, P. Srinivasan, D. Koller, S. Thrun, J. Rodgers, and J. Davis, "SCAPE: Shape completion and animation of people," *ACM Trans. Graph.*, vol. 24, no. 3, pp. 408–416, 2005.

[14] M. Moakher and P. G. Batchelor, "Symmetric positive-definite matrices: From geometry to applications and visualization," *Vis. Process. Tensor Fields*, 2006, pp. 285–298.

[15] M. Calvo and J. M. Oller, "A distance between multivariate normal distributions based in an embedding into the Siegel group," *J. Multivariate Anal.*, vol. 35, no. 2, pp. 223–242, Nov. 1990.

[16] M. Han and F. C. Park, "DTI segmentation and fiber tracking using metrics on multivariate normal distributions," *J. Math. Imag. Vis.*, vol. 49, no. 2, pp. 317–334, Jun. 2014.

[17] N. Boumal, B. Mishra, P. A. Absil, and R. Sepulchre, "Manopt, a Matlab toolbox for optimization on manifolds," *J. Mach. Learn. Res.*, vol. 15, pp. 1455–1459, 2014.

[18] M. Ye, Y. Shen, C. Du, Z. Pan, and R. Yang, "Real-time simultaneous pose and shape estimation for articulated objects using a single depth camera," *IEEE Trans. Pattern Anal. Mach. Intell.*, vol. 38, no. 8, pp. 1517–1532, Aug. 2016.

[19] H. Karcher, "Riemannian center of mass and mollifier smoothing," *Commun. Pure Appl. Math.*, vol. 30, no. 5, pp. 509–541, Sep. 1977.

[20] M. Grant and S. Boyd, "CVX: Matlab software for disciplined convex programming," version 2.0 beta, Sep. 2013. [Online]. Available: http://cvxr.com/cvx

[21] F. C. Park and S. R. Ploen, "A Lie group formulation of robot dynamics," *Int. J. Robot. Res.*, vol. 14, no. 6, pp. 609–618, 1995.

[22] B. Siciliano and O. Khatib, *Handbook of Robotics*. Berlin, Germany: Springer-Verlag, 2008.

[23] C. Davis, "All convex invariant functions of Hermitian matrices," *Archiv der Mathematik*, vol. 8, no. 4, pp. 276–278, 1957.